Optics Letters

Deep turbulence effects mitigation with coherent combining of 21 laser beams over 7 km

Thomas Weyrauch,[1,*] Mikhail Vorontsov,[1,2] Joseph Mangano,[3] Vladimir Ovchinnikov,[2] David Bricker,[2] Ernst Polnau,[1] and Andrey Rostov[2]

[1]Intelligent Optics Laboratory, School of Engineering, University of Dayton, 300 College Park, Dayton, Ohio 45469-2951, USA
[2]Optonicus, 711 E. Monument Avenue, Suite 101, Dayton, Ohio 45402, USA
[3]DARPA/MTO, 675 North Randolph Street, Arlington, Virginia 22203-2114, USA
*Corresponding author: thomas.weyrauch@udayton.edu

Received 3 November 2015; revised 22 December 2015; accepted 7 January 2016; posted 7 January 2016 (Doc. ID 253227); published 12 February 2016

We demonstrate coherent beam combining and adaptive mitigation of atmospheric turbulence effects over 7 km under strong scintillation conditions using a coherent fiber array laser transmitter operating in a target-in-the-loop setting. The transmitter system is composed of a densely packed array of 21 fiber collimators with integrated capabilities for piston, tip, and tilt control of the outgoing beams wavefront phases. A small cat's-eye retro reflector was used for evaluation of beam combining and turbulence compensation performance at the target plane, and to provide the feedback signal for control of piston and tip/tilt phases of the transmitted beams using the stochastic parallel gradient descent maximization of the power-in-the-bucket metric.

OCIS codes: (010.1080) Active or adaptive optics; (140.3298) Laser beam combining; (010.3310) Laser beam transmission.

http://dx.doi.org/10.1364/OL.41.000840

It is well recognized that in strong scintillation conditions typical for propagation over horizontal and slant atmospheric propagation paths near the ground, conventional laser beam projection systems that utilize monolithic aperture telescopes and adaptive optics (AO) wavefront shaping with deformable mirrors (DMs) are not efficient [1–5]. In this Letter, we report experimental results demonstrating efficient laser beam projection and turbulence effects mitigation under conditions of strong scintillations using target-in-the-loop (TIL) coherent combining (phasing) of 21 beams that are generated in a coherent fiber array laser system.

The first demonstration of laser beam projection and atmospheric turbulence mitigation using the TIL coherent beam combining technique was reported by the authors in proof-of-concept experiments using a fiber array with seven fiber collimators (subapertures) [6]. In the experimental study presented here, we demonstrate the ability of coherent fiber array laser systems to significantly improve the performance of laser beam projection in a wide range of atmospheric turbulence conditions, including the strong intensity scintillation regime.

A schematic of the experimental setting at the transmitter side is shown in Fig. 1. The coherent fiber array laser beam projection system was composed of a multichannel master oscillator/power amplifier (MOPA) subsystem based on polarization-maintaining (PM) fibers and fiber elements, fiber array transmitter, power-in-the bucket (PIB) receivers, and control modules. The fiber-coupled, single-mode and narrow-linewidth laser ($\lambda = 1064$ nm) of the MOPA system was fiber connected to a 1×3 fiber splitter, and further to three integrated 1×8 fiber splitter/phase shifter modules. The phase shifters provided an electrically controlled change of the outgoing beams (beamlets) piston phases over 20π rad. The output fibers of the phase shifters were connected to fiber amplifiers. Through the delivery fibers, the amplified laser beams were delivered to an array of 21 densely packed fiber collimators arranged in three clusters (Optonicus INFA modules [7]) on a hexagonal grid as shown in Fig. 1. The fiber collimator clear aperture diameter (subaperture size) was $d_{\text{sub}} = 33$ mm with a 37 mm distance between the optical axes of adjacent fiber collimators in each cluster. Each fiber collimator included a fiber positioner module that allows controllable x- and y-displacement of the delivery fiber tip over ± 50 μm, which corresponds to ± 0.3 mrad range wavefront tip/tilt control for the beamlet emerging from each fiber collimator [8]. The tip/tilt control was used to provide overlapping of the transmitted beamlets at the target plane, compensation of alignment errors between the fiber collimators, and mitigation of slowly varying turbulence-induced wavefront tilts of the transmitted combined beam [8,9].

Target-in-the-loop feedback control of the outgoing beamlet wavefront piston and tip/tilt phases was based on the target-return PIB signal measured by five optical receivers integrated into the transmitter array, as shown in Fig. 1. The larger aperture receiver at the top center of the array was also used as an imaging system for laser beam pointing. Each optical receiver coupled the incident light into a multimode fiber. The received signals were optically combined at a single photodetector, and

its photo-current was used as the PIB receiver metric, J_R, for the wavefront control system.

The control unit of the beam projection system in Fig. 1 consists of independently operating (nonsynchronized) phase-locking and tip/tilt controllers, which utilize the same PIB receiver metric, J_R, as an input signal. The controllers applied voltages to the fiber-integrated phase shifters and fiber positioner modules. Both controllers employed an iterative stochastic parallel gradient descent (SPGD) algorithm for PIB metric optimization [10,11]. The tip/tilt control iteration rate (3.0×10^3 SPGD iterations per second) was limited by the response bandwidth of the fiber positioner modules, while the iterative control of piston phases was performed at 1.4×10^5 Hz. A single SPGD iteration step in piston phase control is considerably shorter than the double-pass propagation time (46.7 μs for the 14 km round-trip). To account for the roundtrip-related latency, the delayed feedback SPGD control algorithm was used [6,12].

During system operation, the phase-locking controller needed, on average, 200–250 SPGD iterations (dependent on turbulence strength and wind speed) to reach ~80% level in the maximization of the PIB metric, which corresponds to a closed loop convergence time on the order of ~2.0–2.5 ms.

The beam projection system efficiency was evaluated via direct measurement of the target plane PIB metric, J_T, which is proportional to the light power entering the small size (unresolved) aperture of the special cat's-eye setup shown in Fig. 1 (right), located at a distance of $L = 7$ km from the laser transmitter system. The cat's-eye setup was designed to reflect about 90% of the incident light power back to the transmitter plane for sensing of the PIB metric J_R and to pass the remaining optical power for measurement of the PIB metric J_T. The cat's-eye optical system was positioned behind a foam board screen with a circular hole of diameter d_{cat} in the center, as shown in Fig. 1 (right). Note that the entrance pupil diameter of the cat's eye, $d_{\text{cat}} = 14$ mm, was selected to be significantly smaller than the diffraction limited beam size, $d_{\text{dif}} \simeq 6$ cm (calculated for a circular aperture of 23 cm diameter, which circumcircles the transmitter array). The short-wave infrared target–plane camera equipped with a wide-angle objective was used to record sets of 250 short-exposure (~2.0 ms exposure time) irradiance distributions of the combined beam projected onto the retro-target at a rate of 30 frames per second.

The atmospheric propagation path geometry was described in [12]. A commercial boundary layer scintillometer (Scintec BLS2000) was used for turbulence characterization. The scintillometer data (instantaneous values of the refractive index structure constant, C_n^2) were averaged during the data recording time (~10 min) for each beam combining experimental trial. The strength of turbulence-induced intensity scintillations were characterized by the Rytov variance $\sigma_R^2 = 1.23\langle C_n^2\rangle L^{11/6}k^{7/6}$, where $k = 2\pi/\lambda$ and $\langle C_n^2\rangle$ is the refractive index structure constant averaged over the measurement trial duration. Amplitude fluctuations are considered weak if $\sigma_R^2 \ll 1$, moderate if $\sigma_R^2 \approx 0.5$–1.0, and strong if $\sigma_R^2 > 1$ [13].

Characteristic examples of the atmospheric-averaged (long-exposure) target–plane irradiance patterns without (a) and with (b–d) SPGD feedback control under different atmospheric conditions are presented in Fig. 2. Each irradiance distribution was obtained by averaging 250 short-exposure frames recorded at a rate of 30 frames per second. The irradiance pattern in Fig. 2(a) corresponds to the incoherent combination of 21 beamlets (phase-locking controller is OFF). The darker spot in the middle of the combined beam footprint represents the hole in the screen with the cat's eye retro-reflector behind. With both controllers (phase-locking and tip/tilt) turned on, we observed the projected combined beam concentration inside a central spot of diameter ~6.5–8.0 cm (dependent on turbulence strength) and the appearance of the side lobes characteristic for coherent beam combining using a multi-aperture laser transmitter. These side lobes were clearly visible under weak-to-moderate turbulence conditions in Fig. 2(b), but became less evident with turbulence strength increased in Fig. 2(c), and practically vanished under strong turbulence conditions in Fig. 2(d).

This decline of the side lobes' visibility with rise of turbulence strength can be explained by the shrinkage of the isoplanatic patch as turbulence strength increases. Indeed, at weak turbulence, phasing of beamlets inside the cat's-eye aperture area leads to the preservation of the beamlets' phase relationship inside the entire isoplanatic area, including the side lobes. With turbulence strength increasing, the side lobes may be outside the isoplanatic patch, which is reduced in size and, hence, beamlets at the side lobes' locations are no longer in phase.

For a more quantitate evaluation of the coherent beam combining performance, compare the evolution curves of the target–plane PIB metric, $J_T(t)$, shown in Fig. 3. They were obtained during an experimental trial with the phase-locking controller sequentially turned ON $[J_T^{\text{ON}}(t)]$ and OFF $[J_T^{\text{OFF}}(t)]$. In this experiment, the TIL fiber array phasing

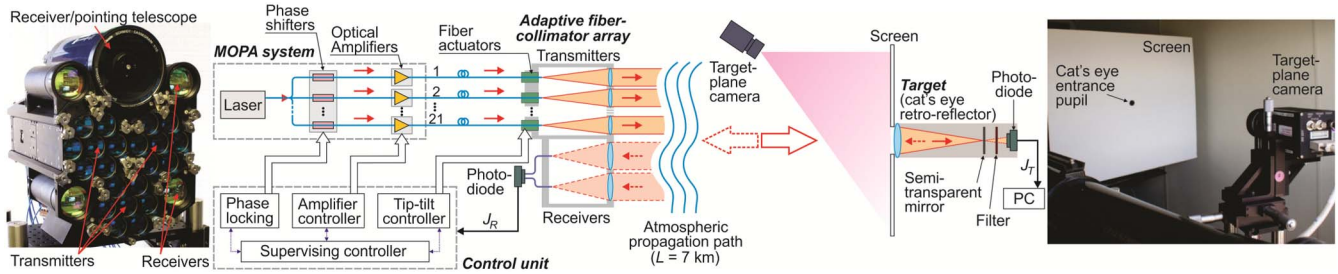

Fig. 1. Experimental settings for analysis of turbulence effects mitigation using adaptive control of piston and tip/tilt phases of multiple (21) laser beams generated in the coherent fiber array transceiver. From left to right: photo of the fiber array laser transceiver, the beam forming system schematic, the target–plane cat's-eye setup schematic, and a photo of the scoring camera in front of the 100 × 80 cm screen. The cat's eye optical setup is located behind a hole in the screen, which defines the cat's-eye system entrance pupil and includes a semi-transparent mirror in the focal plane of a lens and a narrow-linewidth filter in front of a photodiode connected to a PC.

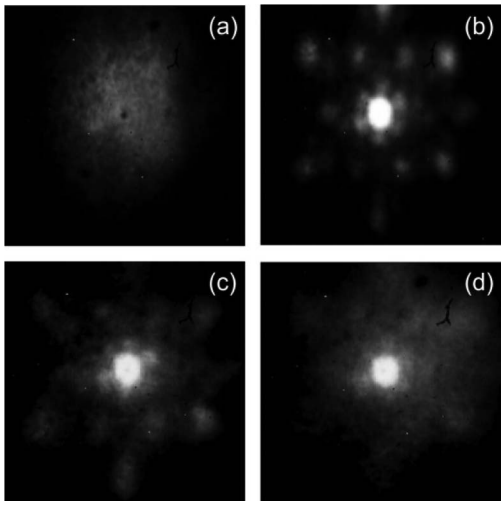

Fig. 2. Atmospheric-averaged irradiance distributions on the target–plane screen (58 cm × 58 cm area) as seen by the target–plane camera with the SPGD phase control off (a) and on (b), (c), and (d): $\langle C_n^2\rangle = 8.6\times10^{-16}$ m$^{-2/3}$ and $\sigma_R^2 = 0.94$ in (a) and (b), $\langle C_n^2\rangle = 1.6\times10^{-15}$ m$^{-2/3}$ and $\sigma_R^2 = 1.8$ in (c), $\langle C_n^2\rangle = 2.5\times10^{-15}$ m$^{-2/3}$ and $\sigma_R^2 = 2.7$ in (d).

resulted in an increase of the PIB metric by a factor of 16 (on average) and a decrease in the normalized variance of the metric fluctuations by a factor of 12 (from 0.73 to 0.06).

The efficiency of turbulence effect mitigation by coherent beam combining under different atmospheric turbulence conditions was evaluated by the atmospheric-averaged Strehl ratio $\langle St\rangle$, commonly defined as the ratio of the atmospheric averaged on-axis intensity at the target plane, $\langle I_0\rangle$, to the corresponding diffraction limited value, I_0^{dif} [14].

It can be shown that under the assumption that the target (cat's eye) size, d_{cat}, is significantly smaller than the diffraction-limited beam size, d_{dif}, the averaged Strehl ratio $\langle St\rangle$ can be directly expressed through the experimentally measured time-averaged metrics $\langle J_T^{\text{ON}}\rangle$ and $\langle J_T^{\text{OFF}}\rangle$ as

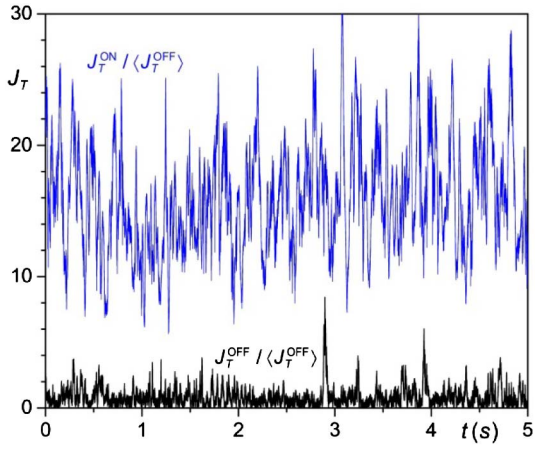

Fig. 3. Time evolution of the normalized PIB metric $J_T(t)$ with the feedback control ON $[J_T^{\text{ON}}(t)]$ and OFF $[J_T^{\text{OFF}}(t)]$. The instantaneous PIB metrics are normalized by the time-averaged value $\langle J_T^{\text{OFF}}\rangle$. The experiment was performed under weak-to-moderate scintillation conditions with $\langle C_n^2\rangle = 6.9\times10^{-16}$ m$^{-2/3}$ and $\sigma_R^2 = 0.75$.

$$\langle St\rangle = \frac{G_{\text{ON/OFF}}}{G_{\text{ON/OFF}}^{\text{VAC}}}\langle St_{\text{beamlet}}\rangle, \tag{1}$$

where $G_{\text{ON/OFF}} = \langle J_T^{\text{ON}}\rangle/\langle J_T^{\text{OFF}}\rangle$ is the gain factor characterizing the increase in the PIB metric value $\langle J_T\rangle$ occurring with TIL phasing of 21 beamlets, $G_{\text{ON/OFF}}^{\text{VAC}}$ is the corresponding ratio of the PIB metrics for propagation in vacuum (theoretically achievable gain factor), and $\langle St_{\text{beamlet}}\rangle$ is the atmospheric-averaged Strehl ratio for a single beamlet. Note that neither $G_{\text{ON/OFF}}^{\text{VAC}}$ nor $\langle St_{\text{beamlet}}\rangle$ can be measured directly due to uncertainties in atmospheric attenuation and variations of the refractive index structure parameter, C_n^2, along the propagation path. For obtaining $\langle St\rangle$ in Eq. (1), we used values $G_{\text{ON/OFF}}^{\text{VAC}}$ and $\langle St_{\text{beamlet}}\rangle$ found through wave optics simulation of the combined beam propagation over 7 km, assuming the Kolmogorov turbulence refractive index power spectrum model and $\langle C_n^2\rangle$ values corresponding to the experimental trial conditions. The fiber array numerical model was described in detail in [12,15].

The experimental results for the gain factor $G_{\text{ON/OFF}}$ and the Strehl ratio $\langle St\rangle$, obtained during a large number of experimental trials performed under different atmospheric turbulence conditions (different $\langle C_n^2\rangle$), are summarized in Fig. 4.

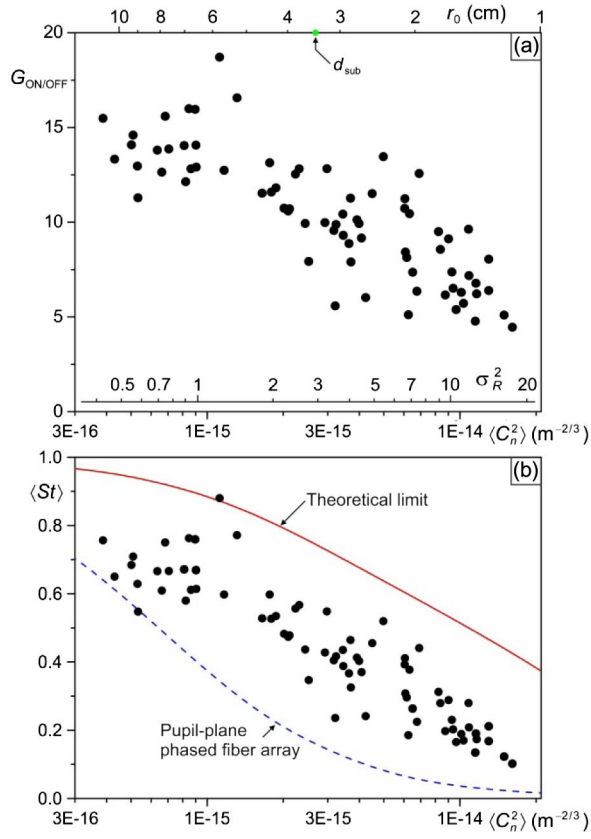

Fig. 4. Experimental results (dots) for (a) the gain factor $G_{\text{ON/OFF}}$ and (b) the Strehl ratio obtained during a number of TIL phase-locking trial over 7 km, under different atmospheric turbulence conditions. The dashed line in (b) corresponds to the fiber array system with pupil–plane phasing, and the solid line corresponds to the theoretically limited Strehl ratio that can be achieved with perfect phase conjugation. The root mean square error in the experimental data (marked by dots) did not exceed 10%.

The plane wave Fried parameter $r_0 = 1.68(C_n^2 L k^2)^{-3/5}$ and the Rytov variance σ_R^2 are provided as additional horizontal axes [top and bottom in Fig. 4(a), respectively]. As seen from the data in Fig. 4(a), TIL phasing resulted in a significant improvement in the beam projection performance by increasing the target PIB metric $\langle J_T \rangle$ by factor of $G_{\mathrm{ON/OFF}}$ between 18 and 12 under turbulence conditions with $\langle \sigma_R^2 \rangle$ ranging from 0.3 to 1.0. With further turbulence and scintillations increase, the gain factor monotonically decreased. Still, even under the most strong scintillations observed in the experiments with $\sigma_R^2 \simeq 18$, TIL phasing of beamlets allowed an up to five-fold increase in the PIB metric. Note that the theoretical maximum for the gain factor in vacuum for the fiber array system used is $G_{\mathrm{ON/OFF}}^{\mathrm{VAC}} \simeq 20$.

The vertical spread of $G_{\mathrm{ON/OFF}}$ values in Fig. 4(a) indicates the variability of results observed in different experimental trials with near equal values of $\langle C_n^2 \rangle$. This variability is related to variations in the transversal wind velocity observed during different experimental trials. The achieved gain factor $G_{\mathrm{ON/OFF}}$ was generally lower in windy conditions.

The efficiency of adaptive mitigation of turbulence-induced distortions via TIL coherent beam combination in terms of the dependency of the Strehl ratio, $\langle St \rangle$, on the turbulence strength (parameter $\langle C_n^2 \rangle$) is illustrated in Fig. 4(b). The experimental data (dots) are shown, along with Strehl ratio curves computed for phased array system models with phasing of beamlets at the pupil plane (no atmospheric compensation) [dashed curve in Fig. 4(b)] and with optimal phase-conjugate pre-compensation, i.e., the theoretically achievable performance limit (solid curve).

It is apparent from Fig. 4(b) that due to adaptive mitigation of turbulence-induced phase aberrations, the TIL phasing can result in a significant improvement in beam projection efficiency if compared with pupil–plane phasing of beamlets, which does not provide atmospheric effect compensation and is only used for mitigation of the MOPA system induced phase noise. This improvement in the Strehl ratio is most noticeable in the strong scintillation regime with Rytov variances ranging from $\sigma_R^2 \cong 1.0$ to $\sigma_R^2 \cong 6.0$, and rapidly decreases with further increase of σ_R^2. Note that conventional adaptive optics enhanced laser beam projection systems can only operate with asignificantly smaller scintillation level (typically not exceeding $\sigma_R^2 \cong 0.3$–0.5) [14].

The decline in the Strehl ratio seen in both the experimental and the numerical simulation results shown in Fig. 4(b) occurs due to a well-known physics reason–the principle impossibility to mitigate the impact of spatially distributed (volume) turbulence by shaping the outgoing wavefront at a single (transmitter) plane [16].

Among technical constraints that prevented the achievement of a better beam projection performance [closer to the curve for the theoretical limit in Fig. 4(b)] are the limited spatial resolution and speed in wavefront phase shaping of the described fiber array system. For efficient turbulence effects mitigation using piston phase control of the outgoing combined beam, the fiber array subaperture diameter, d_{sub}, should be smaller than the turbulence-induced lateral phase aberrations correlation length (Fried parameter, r_0). As the results in Fig. 4 indicate, the condition $d_{\mathrm{sub}} < r_0$ was only fulfilled in the experimental trials with the structure parameter not exceeding $\langle C_n^2 \rangle \simeq 2.7 \times 10^{-15}$ m$^{-2/3}$. An array with a larger number of densely packed fiber collimators with smaller subaperture diameter d_{sub} is expected to provide better performance in strong scintillation conditions. The efficiency of beam projection also can be improved (especially in the propagation scenarios with fast-changing aberrations) using a faster SPGD phase-locking controller.

In conclusion, we experimentally demonstrated efficient adaptive mitigation of atmospheric turbulence-induced phase aberrations along a 7 km horizontal path in strong scintillation conditions using target-in-the loop coherent combining (phasing) of 21 laser beams transmitted by a coherent fiber array system with adaptive control of piston and tip/tilt phases.

This research was developed with funding from the Defense Advanced Research Projects Agency (DARPA) through the SeaHawk and Excalibur programs. The views, opinions, and findings contained in this Letter are those of the authors and should not be interpreted as representing the official views or policies of the Department of Defense or the U.S. Government.

Funding. Air Force Office of Scientific Research (AFOSR) (FA9550-12-1-0449); U.S. Army Research Laboratory (ARL) (W911NF-11-2-0069, W911NF-12-2-0025); Defense Advanced Research Projects Agency (DARPA) (JR0011-14-C-0108).

REFERENCES

1. C. A. Primmerman, T. R. Price, R. A. Humphreys, B. G. Zollars, H. T. Barclay, and J. Herrmann, Appl. Opt. **34**, 2081 (1995).
2. B. M. Levine, E. A. Martinsen, A. Wirth, A. Jankevics, M. Toledo-Quinones, F. Landers, and T. L. Bruno, Appl. Opt. **37**, 4553 (1998).
3. T. Weyrauch and M. A. Vorontsov, Appl. Opt. **44**, 6388 (2005).
4. J. Notaras and C. Paterson, Opt. Express **15**, 13745 (2007).
5. V. P. Lukin, Appl. Opt. **51**, C176 (2012).
6. T. Weyrauch, M. A. Vorontsov, G. W. Carhart, L. A. Beresnev, A. P. Rostov, E. E. Polnau, and J. J. Liu, Opt. Lett. **36**, 4455 (2011).
7. www.optonicus.com.
8. M. A. Vorontsov, T. Weyrauch, L. A. Beresnev, G. W. Carhart, L. Liu, and K. Aschenbach, IEEE J. Sel. Top. Quantum Electron. **15**, 269 (2009).
9. G. A. Filimonov, M. A. Vorontsov, and S. L. Lachinova, Proc. SPIE **8971**, 897109 (2014).
10. M. A. Vorontsov, G. W. Carhart, and J. C. Ricklin, Opt. Lett. **22**, 907 (1997).
11. M. A. Vorontsov and V. P. Sivokon, J. Opt. Soc. Am. A **15**, 2745 (1998).
12. M. Vorontsov, T. Weyrauch, S. Lachinova, T. Ryan, A. Deck, M. Gatz, V. Paramonov, and G. Carhart, *Coherent Laser Beam Combining*, A. Brignon, ed. (Wiley, 2013), p. 167.
13. L. C. Andrews and R. L. Phillips, *Laser Beam Propagation through Random Media* (SPIE, 1998).
14. F. Roddier, ed., *Adaptive Optics in Astronomy* (Cambridge University, 1999).
15. S. L. Lachinova and M. A. Vorontsov, J. Opt. Soc. Am. A **25**, 1960 (2008).
16. M. C. Roggemann and D. J. Lee, Appl. Opt. **37**, 4577 (1998).